J Physiol (2003), **550.2**, *pp.* 419–429
DOI: 10.1113/jphysiol.2003.040113

www.jphysiol.org

Journal of Physiology

Aquaporin-1 and HCO_3^-–Cl^- transporter-mediated transport of CO_2 across the human erythrocyte membrane

Michael E. Blank and Heimo Ehmke

Institut für Vegetative Physiologie und Pathophysiologie, Universität Hamburg, Martinistrasse 52, D-20246 Hamburg, Germany

Recent studies have suggested that aquaporin-1 (AQP1) as well as the HCO_3^-–Cl^- transporter may be involved in CO_2 transport across biological membranes, but the physiological importance of this route of gas transport remained unknown. We studied CO_2 transport in human red blood cell ghosts at physiological temperatures (37 °C). Replacement of inert with CO_2-containing gas above a stirred cell suspension caused an outside-to-inside directed CO_2 gradient and generated a rapid biphasic intracellular acidification. The gradient of the acidifying gas was kept small to favour high affinity entry of CO_2 passing the membrane. All rates of acidification except that of the approach to physicochemical equilibrium of the uncatalysed reaction were restricted to the intracellular environment. Inhibition of carbonic anhydrase (CA) demonstrated that CO_2-induced acidification required the catalytic activity of CA. Blockade of the function of either AQP1 (by $HgCl_2$ at 65 μM) or the HCO_3^-–Cl^- transporter (by DIDS at 15 μM) completely prevented fast acidification. These data indicate that, at low chemical gradients for CO_2, nearly the entire CO_2 transport across the red cell membrane is mediated by AQP1 and the HCO_3^-–Cl^- transporter. Therefore, these proteins may function as high affinity sites for CO_2 transport across the erythrocyte membrane.

(Received 27 January 2003; accepted after revision 23 April 2003; first published online 16 May 2003)
Corresponding author H. Ehmke: Institut für Vegetative Physiologie und Pathophysiologie, Universität Hamburg, Martinistrasse 52, D-20246 Hamburg, Germany. Email: ehmke@uke.uni-hamburg.de

Because of its lipophilic nature, it is generally assumed that CO_2 transport across biological membranes occurs by diffusion through the lipid bilayer. The discovery that apical membranes of gastric glands have an extremely low permeability to CO_2 (Waisbren *et al.* 1994) questioned this common view and initiated a quest for additional routes of membrane CO_2 transport. In 1998, Boron and coworkers (Cooper & Boron, 1998; Nakhoul *et al.* 1998) demonstrated that the expression of the water channel aquaporin-1 (AQP1) in *Xenopus* oocyte membranes, which display a low endogenous CO_2 permeability, increased their permeability to CO_2, suggesting that AQP1 may also function as a gas channel (for review see Cooper *et al.* 2002). In addition, studies in human red blood cell membranes showed that blockade of the HCO_3^-–Cl^- transporter by 4,4′-diisothiocyanato-stilbene-2,2′-disulfonic acid (DIDS) reduced the CO_2 permeability of the human red blood cell membrane (Forster *et al.* 1998) indicating that the erythrocyte HCO_3^-–Cl^- transport protein could also be involved in CO_2 exchange (Fig. 1). Interestingly, the function of AQP1 and the HCO_3^-–Cl^- transporter, which make up a large fraction of total erythrocyte membrane protein and cover a substantial portion of its surface, appear to be coupled. The water transport inhibitor *p*-chloromercuriphenyl-sulfonic acid (pCMBS) has been shown to inhibit the binding site of the specific anion exchange inhibitor 4,4'-dibenzoamido-2,2'-disulfonic stilbene (DBDS; Lukacovic *et al.* 1984). Furthermore, red blood cell urea and water transport seem to occur in parallel (Toon & Solomon, 1986; Ojcius & Solomon, 1988). These observations support the concept that water transport may be structurally coupled to other membrane transport processes.

Taken together, these findings raise the question whether CO_2 transport through AQP1 and the HCO_3^-–Cl^- transporter may be a general physiological route for CO_2 exchange (Fig. 1). The aim of this study was to test this hypothesis in human red blood cell membranes, which express AQP1 and the HCO_3^-–Cl^- transporter at very high levels (Jennings, 1984; Denker *et al.* 1988).

METHODS

Ghost preparation

Blood from healthy volunteers (age 22–45 years) was drawn into K^+-EDTA tubes (S-Monovette, Sarstedt, Germany) and immediately subjected to the preparation of ghosts, which was performed according to Dodge *et al.* (1963). Erythrocytes were washed twice prior to haemolysis (lysis in 30 volumes of phosphate buffered saline (PBS), 20 mosmol kg^{-1}, pH = 7.35 ± 0.2). Lysed cells were washed one to three times under the same conditions and then resealed at 37 °C for 1 h in 10 mM PBS, 300 mosmol kg^{-1}, pH = 7.35 ± 0.2. The cells were loaded with 2′,7′-bis(carboxyethyl)-5(6)-carboxyfluorescein (BCECF) by incubation with the corresponding acetoxymethyl ester (BCECF-AM) for 30 min. Dye-loaded ghosts were washed twice, suspended in 25 volumes PBS, and routinely analysed for concentration of haemoglobin in a Beckman DU 70 spectrophotometer (Beckman Instruments Inc.,

USA). Supernatants were assayed for haemoglobin and BCECF to control cell leakiness. Possible leakage of dye from the ghosts was also checked for by (i) evaluating the signal to noise ratio with time and (ii) by following the emission signal (at 530 nm) with excitation at 440 nm. Neither method indicated substantial (⩽ 5 %) leakage of dye from the ghosts. Within the indicated error all signals were stable for periods > 60 min.

All procedures conformed with the Declaration of Helsinki and written informed consent was given by the subjects.

Experimental set-up

Samples (1.5 ml) were incubated in fluorescence cells for 10 min to achieve temperature equilibrium. Except where otherwise stated, the temperature was held at 37 °C. The samples were stirred at fixed speed (950 r.p.m.) and exposed to a constant gas flow at a rate of 2.5 l h^{-1}, which was controlled and set with a calibrated Rotameter (Rota Yokogawa, Germany). The gas passed through a stopper and was blown onto the surface of either a suspension of ghosts in 300 mosmol kg^{-1} PBS or onto plain PBS ('ghost free'), dependent on the type of assay. Tubing, connections and valves were of the capillary type to keep dead space at a minimum. A capillary bore in the stopper granted pressure relief.

Nitrogen (N_2) was used as an inert, non-acidifying gas while carbogen (5 % CO_2, 95 % O_2) was used as a normal gas mixture to acidify the cells. In some experiments lower fractions of CO_2 were administered, which was achieved by compensating a reduced carbogen flow with N_2 to yield a total flow of 2.5 l h^{-1}.

Standard protocol

Samples were gassed with N_2. After an appropriate time (~5–10 min) the inert gas was replaced with carbogen and acidification, as a result of the reaction $CO_2 + H_2O \rightleftharpoons H^+ + HCO_3^-$, was calculated from the fluorescence signals of BCECF. Some of the experiments were performed with a switch back to N_2 after acidification. Replacement of CO_2 with N_2 showed that acidification was reversible but pH recovery was not symmetrical (Fig. 2*A*). This was confirmed by gassing ghost free buffer (Fig. 2*B*). Steady state of the intracellular pH (pH_i) was achieved after ~1 h (Fig. 3) but usually not recorded.

Measurement of fluorescence

Fluorescence was measured in a Hitachi F2000 spectrophotometer (Hitachi Scientific Instruments, Japan). Excitation scans were used to assay for the amount of BCECF in the suspension or solution. Measurement of pH for ratio calibration was performed either by using nigericin (final concentration: 1 μM) in 10 mM phosphate buffered 154 mM potassium chloride (300 mosmol kg^{-1}, pH = 7.4 ± 0.15) on dye-loaded cells or with BCECF (free acid) in PBS. HCl (100 mM) was added in 10 μl steps and the suspension or solution was allowed to equilibrate to provide a stable signal. Then pH was measured and correlated to the ratio of the emission signals at 530 nm with excitation set to 502 and 440 nm, respectively. An excitation wavelength of 502 was chosen after the calculation of average peak excitation of 30 recordings at an emission wavelength of 530 nm. We found that under our experimental conditions peak excitation was 501.6 ± 1.2 nm (n = 30).

No statistically relevant differences could be detected using either calibration method. Curve fitting for non-linear regression gave r^2 values close to 1 (Fig. 4*A*), (BCECF, nigericin, in phosphate buffered potassium chloride: $r^2 > 0.999$ for a sigmoidal fit; $y = a + b/(1+ e^{(-(x-c)/d)})$, with: a = 0.360 ± 0.112, b = 10.515 ± 0.221, c = 7.035 ± 0.011 and d = 0.454 ± 0.015; n = 5).

To assess whether the uncatalysed acidification rate was proportional to the CO_2 fraction in the feeding gas, PBS was gassed with

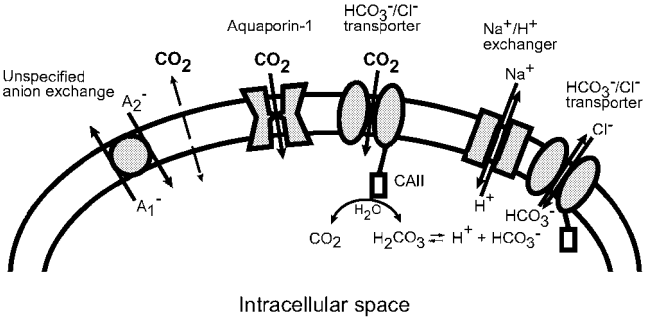

Figure 1. Schematic diagram illustrating possible routes of CO_2 entry into the human erythrocyte and secondary transport processes

CO_2 may enter the erythrocyte either by directly diffusing through the lipid bilayer or by passing through membrane proteins (aquaporin-1, HCO_3^-–Cl^- transporter) which would function as gas channels. Once CO_2 has entered the erythrocyte, it will be hydrated by CAII bound to the carboxyl terminus of the HCO_3^-–Cl^- transporter. Intracellular carbonic acid then dissociates into a proton and bicarbonate. Both reaction products can be eliminated from the intracellular space by specific transporters, the Na^+–H^+ exchanger and the HCO_3^-–Cl^- transporter. These processes will further increase the entry of CO_2 and therefore intracellular acidification. Net proton fluxes may also be linked to anion exchange activity (unspecified anion exchange with substrates A_1^- and A_2^-).

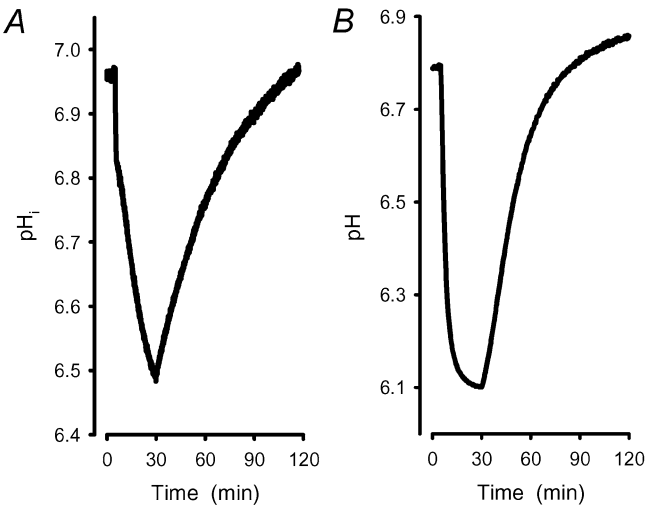

Figure 2. Asymmetry of acidification and pH_i recovery

A, intracellular acidification in ghosts under exposure to carbogen. After 30 min, carbogen was replaced by N_2. The initial pH_i was regained after ~90 min gassing with N_2. The rate of acidification is greater than the rate of pH_i recovery. *B*, recording of an acidification of ghost free buffer (10 mM Tris, pH 6.8). At this pH there is no buffer capacity left in a Tris–HCl buffer system. Therefore the steady state was reached after ~30 min and pH is down to 6.1. Replacement of CO_2 with N_2 also showed an asymmetric pH recovery.

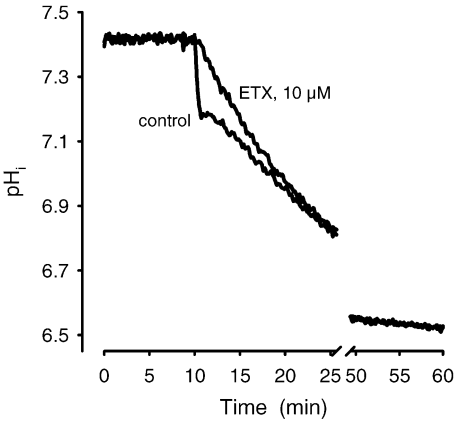

Figure 3. Steady state of pH_i after prolonged exposure to CO_2
Gassing a ghost suspension in PBS with carbogen (control) showed an initial fast acidification and then a slow approach to the physicochemical equilibrium, which was reached after ~60 min. Addition of ETX (10 μM) to the ghost suspension blocked the initial fast component. The physicochemical equilibrium was not affected by the addition of ETX.

different fractions of CO_2 in the gas mixture (5, 4, 3, 2, and 1 %, respectively). Since actually the number of particles or molar amounts of CO_2 had to be considered, values were corrected for pressure and temperature. The equilibration curves for each fraction of CO_2 (Fig. 4*B*) were subjected to regression analysis and revealed regression coefficients with $r^2 > 0.995$ for mono-exponential fits. The resulting velocity constants were plotted as a function of CO_2 and regression analysis was performed again. When assayed for linear relationship the analyses showed regression coefficients indicating a statistical error < 2.5 % (Fig. 4*C*, $r^2 > 0.975$). Fits to sigmoidal equations gave only slightly better coefficients ($r^2 > 0.998$).

Materials

Human carbonic anhydrase II (CAII, E.C. 4.2.1.1), 6-ethoxy-2-benzothiazolesulfon-amide (ETX), *p*-chloromercuriphenyl-sulfonic acid (pCMBS), *p*-chloromercuribenzoic acid (pCMBenzA), and nigericin were obtained from Sigma-Aldrich Co. (Taufkirchen, Germany), 5-(*N*-ethyl-*N*-isopropyl)-amiloride (EIPA) was from Molecular Probes (Eugene, OR, USA) and BCECF, BCECF-AM and 4,4´-diisothiocyanato-stilbene-2,2´-disulfonic acid (DIDS) were obtained from Calbiochem (Bad Soden, Germany). All other chemicals were of analytical grade.

Curve fitting procedures and statistics

Curve fitting was performed using TableCurve by SPSS Inc. Values are expressed as means ± S.D. Statistical evaluation was done by one-way ANOVA followed by the Bonferroni procedure; $P < 0.05$ was taken as the level of significance.

RESULTS

The time course of acidification in control experiments could be dissected into several segments, which, taken separately, could be approximated by quasi first-order functions (Fig. 5). The intracellular pH fell at a high rate immediately after CO_2 flow had been turned on (*a* in

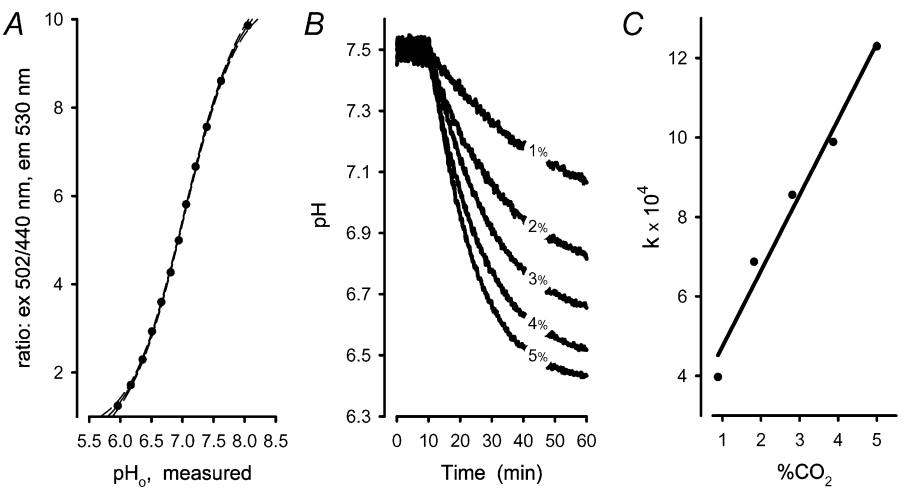

Figure 4. BCECF calibration curve and dependency of acidification rates on the concentration of CO_2
A, BCECF calibration curve measured in a ghost suspension at 1 μM nigericin in 10 mM phosphate buffered potassium chloride (154 mM, 300 mosmol kg^{-1}, pH 7.4 ± 0.15). Data were fitted to a sigmoidal mechanism ($y = a + b/(1+e^{(-(x-c)/d)})$), with $r^2 > 0.999$. Filled circles: pH_o, measured; continuous line: fit results; dashed lines: 95 % confidence. *B*, recordings of acidification in ghost free buffer with ~1, 2, 3, 4 and 5 % CO_2 in the feeding gas. Values corrected for density differences were 0.884, 1.82, 2.81, 3.87, and 5 % CO_2, respectively. *C*, rates of acidification were obtained by fitting the recordings of acidification (*B*) to a mono exponential mechanism. Filled circles: calculated velocity constants (*k*) of a mono-exponential fit; continuous line: linear regression curve ($r^2 > 0.975$).

Fig. 5). Average velocity constant derived from a mono-exponential fit to the fast component of the acidification curve ($k_{in,a}$) was $(3.71 \pm 0.93) \times 10^{-2}$ s^{-1} and average decrease in pH after switching from inert to acidifying gas (ΔpH_a) was 0.35 ± 0.09 ($n = 41$). This was followed by a much more slower decrease of pH (*b* in Fig. 5), with velocity constant derived from a mono-exponential fit to the slow component of the acidification curve ($k_{in,b}$) = $(6.40 \pm 2.00) \times 10^{-4}$ s^{-1} ($n = 41$). In ~35 % of the experiments pH transiently returned towards the baseline value after its initial fall, before the second, slower decrease commenced. This indicates that transport processes are activated, which eliminate acid equivalents from the red blood cell.

Data obtained in the presence of the Na^+–H^+ exchange inhibitor EIPA (10 μM) showed that Na^+–H^+ exchange participates to a lesser extent in the elimination of H^+ into the extracellular space. The hindrance of H^+ back flux was not very pronounced but led to a more distinct transient (Fig. 6*C*). The time course of acidification could be fitted with a (horizontally) mirrored Bateman function, to which a mono-exponential (part *b* in Fig. 5) was added. Several experiments ($n = 4$) in which ghosts were resealed in different buffer systems (PBS, Tris–HCl and Mops each at 10 mM) showed that the elimination of acidic equivalents also depends on the availability of the buffer anion to the anion exchanger (PBS > Tris–HCl > Mops). Furthermore, the elimination of acidic equivalents was markedly decreased at lower temperature (25 °C), at which the overshoot was more prominent (Fig. 6*D*).

The second, slower decrease in pH (*b* in Fig. 5) represents the approach to physicochemical equilibrium. A pure approach to the physicochemical equilibrium, without a fast phase, should also result either (1) if ghost-free PBS is gassed according to the standard protocol, or (2) if carbonic anhydrase is blocked, e.g. by adding the carbonic anhydrase inhibitor ETX (10 μM) to the experimental preparation. As shown in Fig. 7, both predictions could be confirmed experimentally ($n = 14$).

The abolition of the fast acidification process by ETX indicates that the catalytic activity of CA is required for the fast component of the pH response. Loading of ghosts under resealing conditions with increasing amounts of human CAII did not significantly affect fast acidification

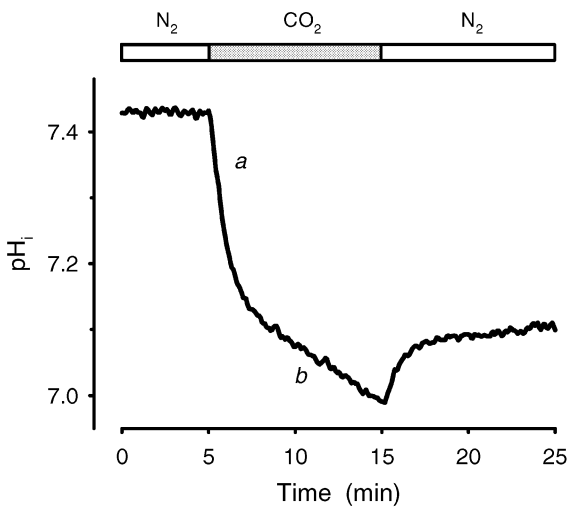

Figure 5. General protocol of an intracellular acidification of a ghost suspension under exposure to CO_2

Acidification was measured with the fluorescent dye BCECF. Excitation wavelengths were set to 502 and 440 nm, emission to 530 nm. The samples (1.5 ml) were incubated in fluorescence cells for 10 min, at 37 °C. Gas flow through a stopper was 2.5 l h^{-1}. The suspension was stirred at 950 r.p.m. First, inert gas (N_2) was used (open bars); then after an appropriate time (here 5 min), gas supply was switched to acidifying gas (carbogen, grey bar). If necessary the cycle was repeated. The graph can be fitted by several mono-exponential functions. *a* denotes the fast process of acidification, *b* the slow approach to physicochemical equilibrium.

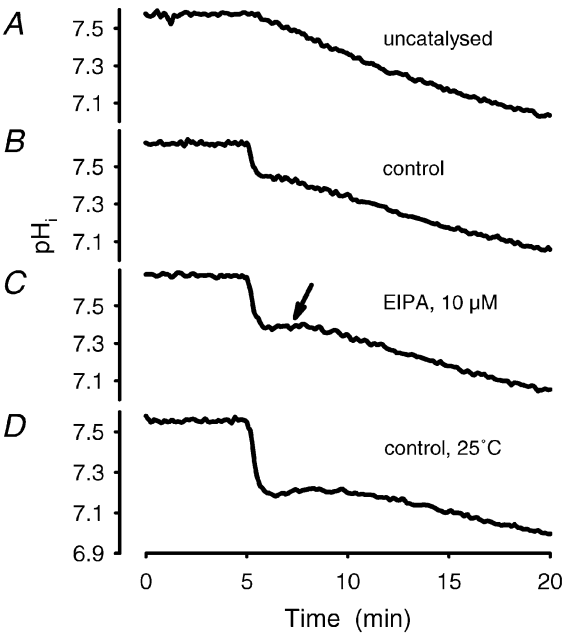

Figure 6. Influence of the proton net back flux capacity on the extent of the fast acidification process

Comparison of the uncatalysed acidification (*A*) with a control assay (*B*) and experiments with retarded back flux (*C* and *D*). The samples were incubated under conditions as described in Fig. 5. *A*, a typical uncatalysed reaction. An uncatalysed reaction is achieved either by adding ETX (10 μM) to the ghost suspension or by gassing PBS to which BCECF (free acid) had been added (see Fig. 7*A* and *B*). *B*, a control experiment, which is the time course of acidification according to the standard protocol. *C*, a retarded back flux under conditions that inhibit the Na^+–H^+ antiporter (10 μM EIPA, incubated for 30 min prior to acidification). The arrow indicates the more pronounced plateau phase (kinetic data of acidification using a mono-exponential fit, see Table 1). *D* demonstrates that a temperature-sensitive transport mechanism is involved in the back flux of acidic equivalents. The temperature was lowered to 25 °C and caused a significant drop in acidification after the onset of CO_2, since the elimination of acidic equivalents is retarded (kinetic data of acidification using a mono-exponential fit, see Table 1).

($n = 3$, see Fig. 8*A*). When CAII was added to either plain PBS buffer or to ghost suspension and subsequently inhibited by ETX, the acidification curves were identical to those of the approach to uncatalysed physicochemical equilibration. The time course and shape were not different from those in Fig. 7*A*. Without inhibition by ETX the assays with CAII added to plain PBS buffer or to ghost suspension showed nearly identical rates of acidification. The acidification rates in the presence of CAII were higher than those of the slow process (*b* in Fig. 9*B*), but they were still considerably lower compared to that of the fast response (*a* in Fig. 9*B*). The same was true if cells in a ghost suspension had undergone lysis by dilution into 6 volumes of hyposmotic (20 mosmol kg^{-1}) buffer (Fig. 8*B*). Data were subjected to curve fitting and gave results with $r^2 > 0.95$ when assayed for bi-exponential mechanisms.

$$y = a + be^{-cx} + de^{-ex},$$

with (1) addition of CAII ($n = 5$):

$a = 6.558 \pm 0.004$, $b = 0.357 \pm 0.150$,
$c = 0.00324 \pm 0.00025$, $d = 0.248 \pm 0.147$,
$e = 0.00149 \pm 0.00022$;

and (2) after lysis ($n = 5$):

$a = 6.540 \pm 0.005$, $b = 0.343 \pm 0.182$,
$c = 0.00293 \pm 0.00050$ $d = 0.303 \pm 0.199$,
$e = 0.00149 \pm 0.00029$.

In the presence of pCMBS (1 mM), which blocks AQP1, we found a moderate decrease in the amount of initial acidification in the range of 10–15 % ($n = 8$), and likewise in the rate constant (Fig. 10 and Table 1). Almost identical results were obtained with the similar chemical pCMBenzA at 1 mM (data not shown). A much more pronounced inhibition than after pCMBS was observed after addition of the AQP1 blocker $HgCl_2$, which completely suppressed the fast process at a concentration of approximately 65 μM. At this concentration of $HgCl_2$ the time course of acidification was identical to that of the chemical equilibrium curve. The IC_{50} of $HgCl_2$ at 37 °C was 39 ± 6 μM ($n = 16$; Fig. 11).

Since $HgCl_2$ has been suggested to slow acidification in reconstituted proteoliposomes by inhibiting CA rather than AQP1 (Yang *et al.* 2000; Fang *et al.* 2002; Verkman, 2002), we measured CAII-catalysed acidification in ghost free PBS in the presence of $HgCl_2$. At 15 μM $HgCl_2$ the rate was slowed down by 1.8 % ($n = 3$, $P > 0.05$), and at 150 μM by 16.6 % ($n = 3$, $P < 0.05$). These results indicate that, at least in our ghost preparation, only a small fraction of the inhibitory effect of $HgCl_2$ on the fast initial acidification can be explained by an inhibition of CAII by $HgCl_2$, because the fast process was already totally blocked at $HgCl_2$ concentrations > 65 μM.

DIDS, an inhibitor of the HCO_3^-–Cl^- transporter, also inhibited the intracellular acidification of red blood cell ghosts exposed to CO_2. The extent of inhibition was concentration dependent (Fig. 12, Table 1) and highly influenced by incubation conditions like duration and exposure to light sources. (The light-sensitive compound was also sensitive to photometric light.) The fast process was completely abolished after 15 min of incubation at a

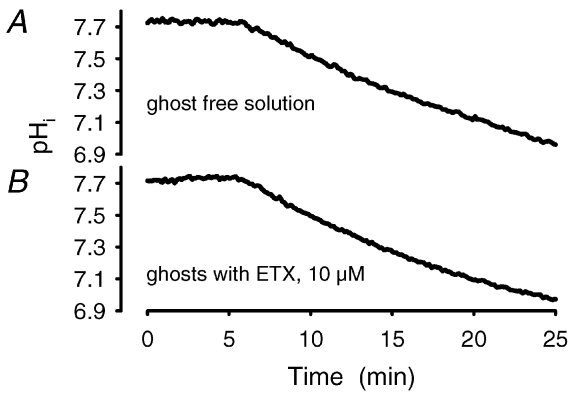

Figure 7. Gassing of ghost-free buffer and gassing CAII-blocked ghost suspensions reveal identical time courses

Approach to the physicochemical equilibrium: comparison of the time course of acidification of uncatalysed reactions. *A*, time course of a ghost-free buffer (PBS: 10 mM, 300 mosmol kg^{-1}, pH: 7.4) solution to which BCECF (free acid) has been added. *B*, typical time course of acidification with blocked CAII activity through addition of the membrane-permeant ETX (10 μM). The time constants of both assays were not statistically different.

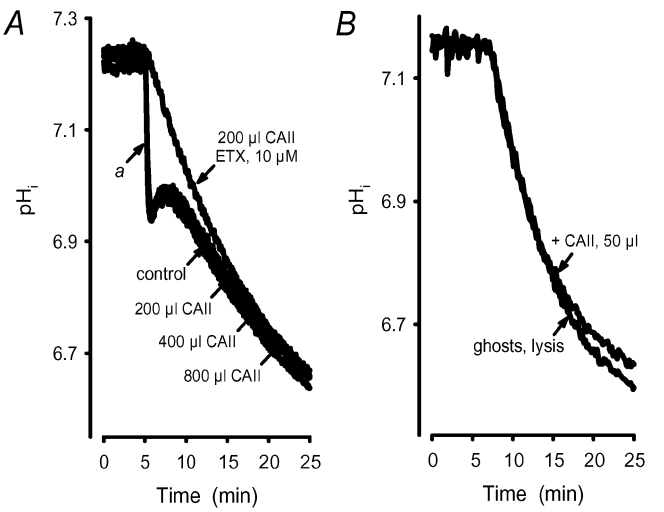

Figure 8. CAII activity in a ghost preparation is not rate limiting under experimental conditions

A, under the condition of resealing, ghosts were incubated with different amounts of human CAII (0, 200, 400 and 800 μl of 2.5 mg ml^{-1} CAII). *a* denotes the fast acidification for the four assays. The statistical error of the initial rates is < 5 %, i.e. CAII load of a ghost preparation does not increase the rate or the ΔpH_i of the fast acidification. *B*, the rate of acidification after addition of CAII (50 μl) to a ghost suspension was very similar to the rate of acidification calculated for ghosts that had undergone lysis by a 1:6 dilution into hyposmotic (20 mosmol kg^{-1}) PBS.

Table 1. Effects of experimental interventions on the time course of intracellular acidification

	ΔpH_a (% of control)	$k_{in,a}$ (% of control)	$k_{in,b}$ (% of control)	*n*
Control (25 °C)	199 ± 18 *	77 ± 6 *	65 ± 27 *	7
EIPA (10 μM)	131 ± 16 *	98 ± 13	112 ± 20	8
PCMBS (1 mM)	85 ± 10 *	87 ± 6 *	76 ± 9 *	8
DIDS (1.5 μM)	74 ± 7 *	89 ± 10 *	96 ± 12	25
DIDS (7.5 μM)	30 ± 5 *	102 ± 12	123 ± 12 *	25
DIDS (15 μM)	n.d.	n.d.	213 ± 25 *	25

Quantitative analysis of the effects of temperature (25 °C), pharmacological blockade of the Na^+–H^+ transporter (EIPA), pharmacological blockade of AQP1 (PCMBS), and pharmacological blockade of the HCO_3^-–Cl^- transporter (DIDS). ΔpH_a represents the initial rapid decrease in pH after switching from inert to acidifying gas. Values were derived from a curve fit to a mono-exponential mechanism and are given as relative change from the paired control assay. $k_{in,a}$ represents the velocity constant derived from a mono-exponential fit to the fast component of the acidification curve (see *a* in Fig. 5), expressed as relative value of the paired control assay; $k_{in,b}$ represents the velocity constant derived from a mono-exponential fit to the slow component of the acidification curve (see *b* in Fig. 5), expressed as relative value of the paired control assay. n.d., not determined; *n*, number of experiments; * $P < 0.05$ *vs.* control.

DIDS concentration of 15 μM ($n = 25$; IC_{50}: 5.6 ± 1.2 μM). Inhibition by DIDS was temperature sensitive, but to a lesser extent than that by $HgCl_2$ (data not shown).

At 37 °C, a combination of DIDS (10 μM) and $HgCl_2$ (40 μM) completely blocked fast acidification (3–5 % ghost-volume; $n = 11$, Fig. 13). If DIDS was administered first, the drop of the fluorescence ratio, which occurred immediately after the addition of $HgCl_2$, did not recover completely within the next 10–15 min (*b* in Fig. 13*C*). Regaining of a normal pH is obviously linked to a high capacity exchange mechanism, which can be inhibited with DIDS (Gros & Moll, 1974; Gros *et al.* 1976; Bisognano *et al.* 1993).

The net H^+ flux capacity of ghost preparations was assessable by analysing the time course of pH recovery

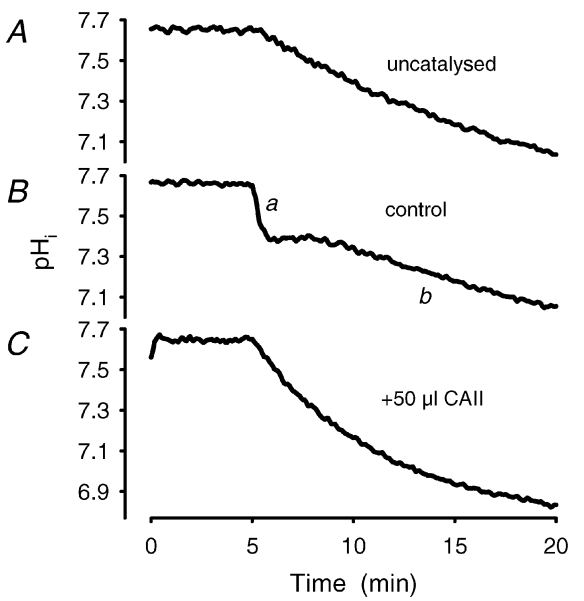

Figure 9. Intracellular CAII is required for fast and biphasic acidification

Addition of CAII (50 μl of 2.0 mg ml^{-1} human CAII) to the extracellular compartment of a ghost suspension (*C*) yields higher rates than the uncatalysed approach to the physicochemical equilibrium (*A*) (by addition of 10 μM ETX to the ghost suspension). No difference from Fig. 6*A* and Fig. 7*B* regarding the velocity constants could be detected. *B*, a control experiment with a fast (*a*) and a slow (*b*) acidification response.

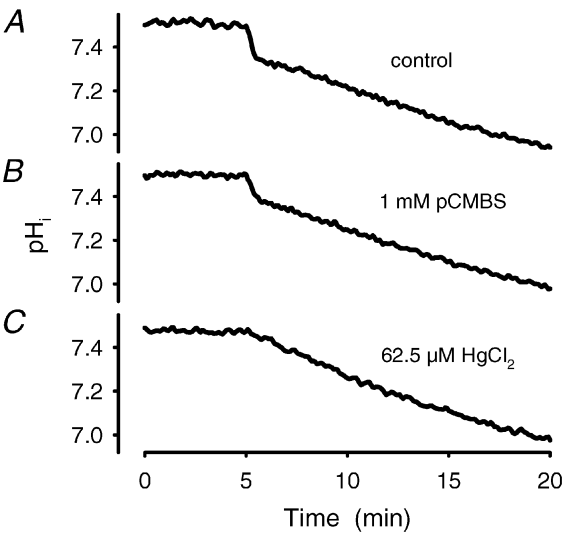

Figure 10. Comparison of the effect of the AQP1 blocker pCMBS and $HgCl_2$

A, a control experiment. *B*, the sample has been incubated for 15 min with pCMBS at a final concentration of 1 mM. The change of pH in the fast phase is less and the time constant of that process is smaller compared to control. *C* represents the time course of an acidifying process measured in ghosts with $HgCl_2$ at a concentration of 62.5 μM. After onset of CO_2 the time course is not distinguishable from an uncatalysed reaction.

after acidification of ghosts with the sodium salt of propionic acid (30 mM). Immediately after the compound was added to a ghost suspension a significant drop of the pH in the intracellular space was recorded. The pH recovery was determined at temperatures between 4 and 37 °C (data not shown) and fitted to bi-exponential equations. Both exponential terms of the regression analysis were characterized by low activation energy in the range of 2.2 to 4.5 kcal mol^{-1} (9.2–18.8 kJ mol^{-1}). EIPA (10 μM) suppressed the rate of pH recovery after acidification by 15 % ($P < 0.05$, $n = 3$), while DIDS (15 μM) caused a 80 % inhibition ($P < 0.05$, $n = 3$) (data not shown). These experiments confirm that only a small portion of net H^+ flux across the membrane was mediated by the Na^+–H^+ exchanger.

To rule out that fast acidification processes as recorded with intracellular BCECF could be the result of a fast extracellular formation of protons, which would then be transported into the intracellular space (Norris & Powell, 1992), we compared rates of acidification inside to outside the cells. To measure proton concentration in the extracellular environment we used a ghost preparation as described in Methods except that the cells were not loaded with dye. Membrane-impermeant BCECF (free acid) was then added to this cell suspension. In contrast to an intracellular acidification caused by the addition of sodium propionate (30 mM) no significant change in proton concentration could be detected outside the cells (data not shown). All experiments with fluorescence indicator in the extracellular compartment that followed the standard protocol including those in the presence of the inhibitors DIDS and/or $HgCl_2$ resulted in a time course of acidification with time constants identical to those of the uncatalysed reaction ($P < 0.05$; $n = 18$, Fig. 13*B*, *D* and *F*).

DISCUSSION

The results of the studies presented here with inhibitors of integral erythrocytic proteins indicate that, at low partial pressure differences, a major part of CO_2 entry into red blood cell ghosts is dependent on an intact structure and/or function of the HCO_3^-–Cl^- transporter and AQP1. Thus, these proteins may function as high affinity sites for CO_2 transport across the erythrocyte membrane (see Fig. 1).

The fast component of the intracellular acidification response, which describes the rapid CO_2 entry into the red blood cell, was completely suppressed if the concentration of DIDS was kept high enough to inhibit any anion exchange activity of the HCO_3^-–Cl^- transporter. Under these conditions the entire intracellular acidification

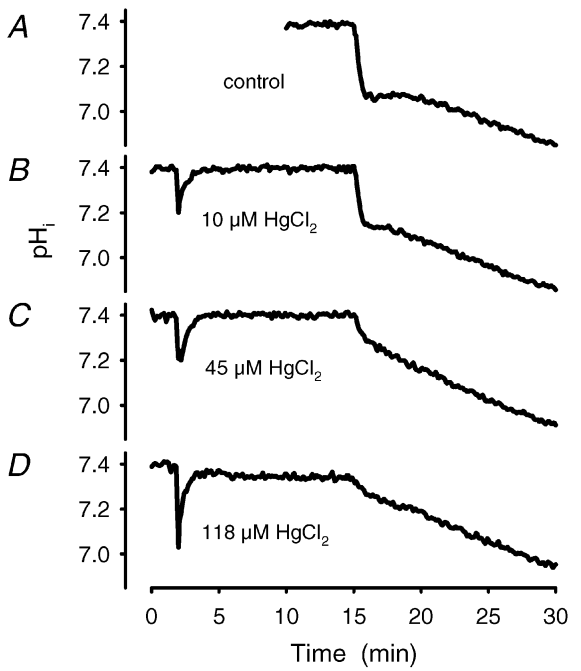

Figure 11. Establishment of a dose–response curve for the AQP1 inhibitor $HgCl_2$

A dose–response curve has been derived from acidification experiments in the presence of various concentrations of $HgCl_2$. Incubation time was 13 min. *A*, control with vehicle (PBS) added. *B*, time course at 10 μM $HgCl_2$. *C*, time course at 45 μM $HgCl_2$ and *D*, at 118 μM $HgCl_2$. The IC_{50} calculated from the velocity constants was 39 ± 6 μM, $n = 16$.

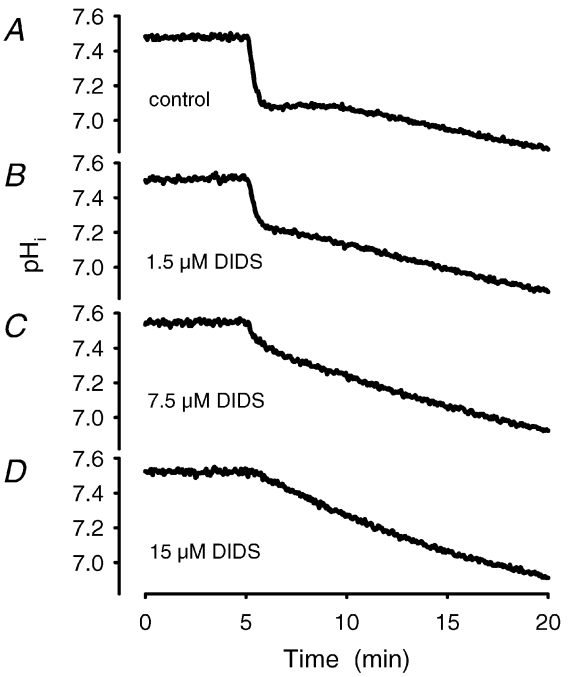

Figure 12. Establishment of a dose–response curve for the HCO_3^-–Cl^- transport inhibitor DIDS

A dose–response curve has been derived from acidification experiments in the presence of various concentrations of DIDS. The time course of acidification was registered after incubation with DIDS for 10 min. *A*, control with vehicle (PBS) added. *B*, time course at 1.5 μM DIDS. *C*, time course in the presence of 7.5 μM DIDS and *D*, at 15 μM DIDS. The IC_{50} calculated from the velocity constants was 5.6 ± 1.2 μM, $n = 25$.

followed the uncatalysed approach to the physicochemical equilibrium. This effect of DIDS was not due to an inhibition of CA, as shown in separate experiments in which human CAII was added to ghost-free PBS. To confirm that an intact function of the HCO_3^-–Cl^- transporter is required for the fast acidification process, we performed experiments with the most potent known inhibitor of the HCO_3^-–Cl^-transporter, the oxonol dye bis(1,3-dibutyl-barbituric acid)pentamethine oxonol (diBA) (Knauf *et al.* 1995). At 15 μM diBA completely suppressed the fast acidification process (data not shown). Since the inhibitors DIDS and diBA are not competing for the same binding site (Knauf *et al.* 1995), it is very likely that both cause specific conformational changes in the protein strong enough to hinder the passage of CO_2.

It has been discussed that DIDS may disturb the lipid bilayer directly (Forster *et al.* 1998) and thus reduce membrane permeability of CO_2. From the present experiments it cannot be excluded that DIDS may interact with the lipid bilayer. However, the estimated number of molecules per cell in our assays in the case of a complete inhibition of the fast acidification response argues for a specific effect on the HCO_3^-–Cl^- transporter: a fraction of 5 % ghosts in 1.5 ml PBS, ~90 fl of mean ghost volume and a concentration of DIDS of 15 μM result in $\sim 16 \times 10^6$ molecules per cell. With $\sim 1.5 \times 10^6$ copies of HCO_3^-–Cl^- transporter per cell (Ship *et al.* 1977) and assuming no other binding sites for DIDS, this corresponds to a number of ~10 inhibitor molecules per HCO_3^-–Cl^- transporter protein. Considering the size and chemical properties of DIDS it seems unlikely that these few molecules could have a profound effect on the lipid bilayer in such a way that a lipophilic compound would be completely hindered from passing through the lipids.

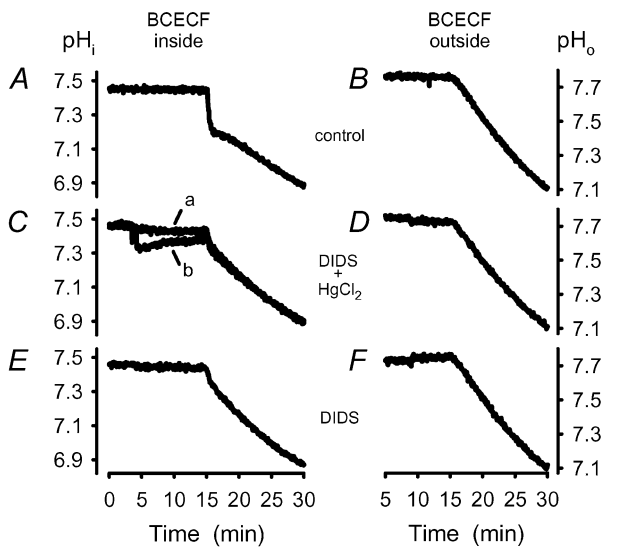

Figure 13. Comparison of acidification in the intracellular and extracellular compartment in control and inhibition experiments

Fluorescence inside the cell was measured as usual on BCECF-loaded cells. To measure outside the cells, ghosts were used that were not loaded with dye and added membrane-impermeant BCECF (free acid) to the outer compartment. *A*, control experiment (vehicle: PBS). *B*, same as *A* but with BCECF outside the cells. *C*, *a*, $HgCl_2$ (10 μM) was added prior to DIDS (8 μM); *b*, DIDS (8 μM) was added prior to $HgCl_2$ (10 μM). *D*, same as *C a*, but with BCECF outside the cells. *E*, DIDS (10 μM) present in the preparation, incubation 10 min. *F*, same as *E*, but with BCECF outside the cells.

Inhibition of the fast acidification by DIDS could possibly also be explained by a blockade of HCO_3^- extrusion out of the red blood cell (Sterling *et al.* 2001*a*,*b*). In this case, CO_2 would enter the cell through the lipid bilayer where intracellular CA converts it to H^+ and HCO_3^-. The anion would then serve as a substrate for the HCO_3^-–Cl^- transporter and the proton would remain in the cell, thus acidifying it. An inhibition of the HCO_3^-–Cl^-transporter, e.g. by DIDS, would then slow down this process through a feedback mechanism (see Fig. 1). It seems, however, rather unlikely that blockage of HCO_3^- extrusion will suppress any rate of acidification faster than the pure approach to the physicochemical equilibrium. Since we did not detect any non-passive acidification at 15 μM DIDS we would favour the idea that DIDS is inhibiting fast acidification by hindrance of CO_2 entry into the cells, either across the HCO_3^-–Cl^- transporter itself, or through a membrane pathway which requires a functionally intact HCO_3^-–Cl^-transporter.

Inhibition of AQP1 by the mercuric compounds pCMBS and $HgCl_2$ also inhibited rapid intracellular acidification. This indicates that in the human erythrocyte membrane AQP1 functions as a gas channel (see Fig. 1), confirming previous observations on cloned AQP1 protein expressed in *Xenopus* oocytes (Cooper & Boron, 1998; Nakhoul *et al.* 1998) and on reconstituted AQP1 in proteoliposomes (Prasad *et al.* 1998). While both inhibitors target the same chemical group (sulfhydryl group of cysteine), $HgCl_2$ proved to be > 100-fold as potent as pCMBS. A possible explanation of this difference is that the inhibition of AQP1 by pCMBS requires an intact cytoskeleton (Ojcius *et al.* 1988), e.g. by making or keeping specific binding site(s) available to the inhibitor. Since haemoglobin participates in the normal structure of the red blood cell cytoskeleton, the cytoskeleton is probably organized in a different way in ghosts compared to intact red blood cells. As a consequence the availability of binding sites to pCMBS may be severely impaired in ghosts. This may also explain why rapid acidification induced by CO_2 was only moderately impaired (10–15 %) at a concentration of pCMBS (1 mM) which completely blocks AQP1 mediated water flux in red blood cells (Preston *et al.* 1992). Since the CO_2 molecule is linear and its cross-sectional area is considerably smaller than that of the water molecule, a

passage of CO_2 may still occur with a partial block of AQP1 by pCMBS at a concentration which on the other hand is sufficient to completely prevent the transport of water through the protein pore.

At 37 °C the fast acidification of a 5 % ghost suspension was found to be completely suppressed in the presence of ~65 μM $HgCl_2$, which results in $\sim 70 \times 10^6$ molecules per cell. If $HgCl_2$ would only bind to AQP1, which has one binding site for $HgCl_2$ and is present at a total number of $\sim 0.25 \times 10^6$ copies per cell, this concentration would yield 280 molecules of inhibitor per AQP1. $HgCl_2$, however, shares chemical binding characteristics with pCMBS, which has been shown to bind to six reactive sulfhydryl groups of the HCO_3^-–Cl^- transporter (Lukacovic *et al.* 1984). Given a total estimate of $\sim 1.5 \times 10^6$ molecules of the HCO_3^-–Cl^- transporter per cell and similar binding constants of $HgCl_2$ for AQP1 and the HCO_3^-–Cl^- transporter, this results in a corrected number of ~10–12 molecules per AQP1 binding site. This number is in the same low range as that for DIDS. Importantly, previous studies indicate that the reaction of pCMBS with sulfhydryl groups of the HCO_3^-–Cl^- transporter has no effect on its anion exchange activity (Zhang & Solomon, 1992). Accordingly, the interaction of $HgCl_2$ with integral ghost proteins may be rather specific to impair the function of AQP1 (Preston *et al.* 1992, 1993).

Interestingly, sub-maximal concentrations of both inhibitors were sufficient to completely inhibit fast acidification, when they were administered concurrently. This observation supports the concept of a close interaction between the HCO_3^-–Cl^- transporter and AQP1 in CO_2 transport.

Thus, AQP1 and the HCO_3^-–Cl^- transporter may be part of or form a molecular complex that bundles metabolic processes, hence forming a functional complex that optimizes CO_2 transport across the erythrocyte membrane. The concept of such a complex is also supported by results obtained with the phlorizin analogue *p*-azidobenzylphlorizin (pAzBenzPhz), which selectively photolabels AQP1 and the HCO_3^-–Cl^- transporter of the human red blood cell (Hoefner *et al.* 1997) without inserting significantly into the membrane (Wyse *et al.* 1988). Labelling of AQP1 is enhanced in the presence of DIDS and suppressed competitively by the mercuric compounds pCMBS and $HgCl_2$ (Hoefner *et al.* 1997).

Addition of CAII to the extracellular space of an intact ghost suspension caused higher rates of intracellular acidification than that of the approach to the physicochemical equilibrium (Fig. 9*A* and *C*) but rates were still slower than those of the normal fast response (*a* in Fig. 9*B*). This observation may be explained by an accelerated H^+ exchange if CAII is present in the intracellular space. The low activation energy (< 4.5 kcal mol^{-1}; < 18.8 kJ mol^{-1}) we calculated for pH recovery after acidification with sodium propionate (see Results) would be in favour of such a fast mechanism. The fact that in the presence of DIDS (15 μM) the rate of pH recovery was suppressed by 80 % suggests that the HCO_3^-–Cl^- transporter participates in the pH recovery (Gros *et al.* 1976).

An important question is how CA activity remains in the ghost preparation, even though the cells have been lysed. The preparation of ghosts was performed with the same technique as described by Dodge *et al.* (1963). Spectrophotometric measurements (see Methods) demonstrated that in the present study most preparations contained some haemoglobin. Most previous investigations did not detect CA activity in ghosts (Enns, 1967; Rosenberg & Guidotti, 1968; Tappan, 1968; Randall & Maren, 1972), but recently it could be demonstrated that CAIV is localized on the extracellular surface of human erythrocytes (Wistrand *et al.* 1999). Moreover, CAII can bind to the carboxyl terminus of the HCO_3^-–Cl^- transporter (Vince & Reithmeier, 1998), suggesting that at least a fraction of the highly active CAII is still associated with the membrane of the ghost preparation. This interpretation is supported by the observation that adding the membrane-permeant CA inhibitor ETX (10 μM) reduced any catalysed rate of acidification to the uncatalysed approach towards the physicochemical equilibrium. Finally, preparations of lysed ghosts exhibited high activity of CA, which may be due to the enhanced CA activity in the presence of erythrocyte membranes (Wistrand, 1981; Parkes & Coleman, 1989).

The potential physiological significance of AQP1 and HCO_3^-–Cl^- transporter-mediated CO_2 fluxes remains to be established in further studies. One important limitation is the relative lack of specificity of the chemical blockers used in this study to inhibit protein-mediated CO_2 transport. Moreover, further experiments under equilibrium exchange conditions will be necessary to allow for an adequate calculation of CO_2 permeability in normal erythrocytes. It will be interesting to compare these permeabilities with those measured in erythrocytes from AQP1-deficient mice (Yang *et al.* 2000; Fang *et al.* 2002) or humans carrying a mutation in the AQP1 gene (Preston *et al.* 1994). Such experiments should help to assess whether protein-mediated CO_2 transport across biological membranes may attain a major role under physiological or patho-physiological stress conditions, like heavy exercise, high altitude, or a thickening of the blood–gas barrier.

In summary, we interpret our data in terms of CO_2 exchange across the red blood cell membrane in the following way:

(i) The rate of acidification in a ghost suspension in the presence of a completely inhibited CA activity by ETX is identical to that of the uncatalysed reaction towards the physicochemical equilibrium. Thus, any rate of acidi-

fication greater than that of an uncatalysed reaction requires the catalytic activity of CA.

(ii) The observation, that lysed ghosts and ghosts with CAII added to the extracellular compartment reveal submaximal rates of acidification, suggests that integer membranes and/or complex structures are essential for the fast acidification process in ghosts.

(iii) Measurements with BCECF outside the ghosts yielded acidification rates identical to that of an uncatalysed reaction. Thus, all effects besides the approach to the physicochemical equilibrium are caused by intracellular events.

(iv) The complete inhibition of the fast acidification by $HgCl_2$ and DIDS indicate that the HCO_3^-–Cl^- transporter and APQ1 mediate CO_2 transport over the human red cell membrane.

(v) Thus, at low concentration gradients for CO_2 the HCO_3^-–Cl^- transporter and AQP1 may be considered as high affinity sites and as a main route for CO_2 entry into the human red blood cell.

REFERENCES

Bisognano JD, Dix JA, Pratap PR, Novak TS & Freedman JC (1993). Proton (or hydroxide) fluxes and the biphasic osmotic response of human red blood cells. *J Gen Physiol* **102**, 99–123.

Cooper GJ & Boron WF (1998). Effect of pCMBS on CO_2 permeability of *Xenopus* oocytes expressing aquaporin 1 or its C189S mutant. *Am J Physiol* **275**, C1481–1486.

Cooper GJ, Zhou Y, Bouyer P, Grichtchenko II & Boron WF (2002). Transport of volatile solutes through AQP1. *J Physiol* **542**, 17–29.

Denker BM, Smith BL, Kuhajda FP & Agre P (1988). Identification, purification, and partial characterization of a novel Mr 28,000 integral membrane protein from erythrocytes and renal tubules. *J Biol Chem* **263**, 15634–15642.

Dodge JT, Mitchell C & Hanahan DJ (1963). The preparation and chemical characteristics of hemoglobin-free ghosts of human erythrocytes. *Arch Biochem Biophys* **100**, 119–130.

Enns T (1967). Facilitation by carbonic anhydrase of carbon dioxide transport. *Science* **155**, 44–47.

Fang X, Yang B, Matthay MA & Verkman AS (2002). Evidence against aquaporin-1-dependent CO_2 permeability in lung and kindney of mice. *J Physiol* **542**, 63–69.

Forster RE, Gros G, Lin L, Ono Y & Wunder M (1998). The effect of 4,4′-diisocyocynato-stilbene-2,2′-disulfonate on CO_2 permeability of the red blood cell membrane. *Proc Natl Acad Sci U S A* **95**, 15815–15820.

Gros G & Moll W (1974). Facilitated diffusion of CO_2 across albumin solutions. *J Gen Physiol* **64**, 356–371.

Gros G, Moll W, Hoppe H & Gros H (1976). Proton transport by phosphate diffusion: a mechanism of facilitated CO_2 transfer. *J Gen Physiol* **67**, 773–790.

Hoefner DM, Blank ME & Diedrich DF (1997). The anion transporter and a 28 kDa protein are selectively photolabeled by p-azidobenzylphlorizin under conditions that alter RBC morphology, flexibility, and volume. *Biochim Biophys Acta* **1327**, 231–241.

Jennings ML (1984). Oligomeric structure and the anion transport function of human erythrocyte band 3 protein. *J Membr Biol* **80**, 105–117.

Knauf PA, Law FY & Hahn K (1995). An oxonol dye is the most potent known inhibitor of band 3-mediated anion exchange. *Am J Physiol* **269**, C1073–1077.

Lukacovic MF, Verkman AS, Dix JA & Solomon AK (1984). Specific interaction of the water transport inhibitor, pCMBS, with band 3 in red blood cell membranes. *Biochim Biophys Acta* **778**, 253–259.

Nakhoul NL, Davis BA, Romero MF & Boron WF (1998). Effect of expressing the water channel aquaporin-1 on the CO_2 permeability of *Xenopus* oocytes. *Am J Physiol* **274**, C543–548.

Norris FA & Powell GL (1992). Characterization of CO_2/carbonic acid mediated proton flux through phosphatidylcholine vesicles as model membranes. *Biochim Biophys Acta* **1111**, 17–26.

Ojcius DM & Solomon AK (1988). Sites of p-chloromercuribenzene-sulfonate inhibition of red cell urea and water transport. *Biochim Biophys Acta* **942**, 173–182.

Ojcius DM, Toon MR & Solomon AK (1988). Is an intact cytoskeleton required for red cell urea and water transport? *Biochim Biophys Acta* **944**, 19–28.

Parkes JL & Coleman PS (1989). Enhancement of carbonic anhydrase activity by erythrocyte membranes. *Arch Biochem Biophys* **275**, 459–468.

Prasad GV, Coury LA, Finn F & Zeidel ML (1998). Reconstituted aquaporin 1 water channels transport CO_2 across membranes. *J Biol Chem* **273**, 33123–33126.

Preston GM, Carroll TP, Guggino WB & Agre P (1992). Appearance of water channels in *Xenopus* oocytes expressing red cell CHIP28 protein. *Science* **256**, 385–387.

Preston GM, Jung JS, Guggino WB & Agre P (1993). The mercury-sensitive residue at cysteine 189 in the CHIP28 water channel. *J Biol Chem* **268**, 17–20.

Preston GM, Smith BL, Zeidel ML, Moulds JJ & Agre P (1994). Mutations in aquaporin-1 in phenotypically normal humans without functional CHIP water channels. *Science* **265**, 1585–1587.

Randall RF & Maren TH (1972). Absence of carbonic anhydrase in red cell membranes. *Biochim Biophys Acta* **268**, 730–732.

Rosenberg SA & Guidotti D (1968). The protein of human erythrocyte membranes. *J Biol Chem* **243**, 1985–1992.

Ship S, Shami Y, Breuer W & Rothstein A (1977). Synthesis of tritiated 4,4′-diisothiocyano-2,2′-stilbene disulfonic acid ([3H]DIDS) and its covalent reaction with sites related to anion transport in human red blood cells. *J Membr Biol* **33**, 311–323.

Sterling D, Reithmeier RAF & Casey JR (2001*a*). Carbonic anhydrase: In the driver's seat for bicarbonate transport. *J Pancreas* **2**, 165–170.

Sterling D, Reithmeier RAF & Casey JR (2001*b*). A transport metabolon. Functional interaction of carbonic anhydrase II and chloride/bicarbonate exchangers. *J Biol Chem* **276**, 47886–47894.

Tappan DV (1968). Carbonic anhydrase activity of erythrocyte ghosts. *Experientia* **24**, 127.

Toon MR & Solomon AK (1986). Control of red cell urea and water permeability by sulfhydryl reagents. *Biochim Biophys Acta* **860**, 361–375.

Verkman AS (2002). Does aquaporin-1 pass gas? An opposing view. *J Physiol* **542**, 31.

Vince JW & Reithmeier RAF (1998). Carbonic anhydrase II binds to the carboxyl terminus of human band 3, the erythrocyte Cl^-/HCO_3^- exchanger. *J Biol Chem* **273**, 28430–28437.

Waisbren SJ, Geibel JP, Modlin IM & Boron WF (1994). Unusual permeability properties of gastric gland cells. *Nature* **368**, 332–335.

Wistrand PJ (1981). The importance of carbonic anhydrase B and C for the unloading of CO_2 by the human erythrocyte. *Acta Physiol Scand* **113**, 417–426.

Wistrand PJ, Carter ND, Conroy CW & Mahieu I (1999). Carbonic anhydrase IV activity is localized on the exterior surface of human erythrocytes. *Acta Physiol Scand* **165**, 211–218.

Wyse JW, Blank ME, Maynard CL, Diedrich DF & Butterfield DA (1988). Electron spin resonance investigation of the interaction of the anion and glucose transport inhibitor, p-azidobenzylphlorizin, with the human red cell membrane. *Biochim Biophys Acta* **979**, 127–131.

Yang B, Fukuda N, Van Hoek A, Matthay MA, Ma T & Verkman AS (2000). Carbon dioxide permeability of aquaporin-1 measured in erythrocytes and lung of aquaporin-1 null mice and in reconstituted proteoliposomes. *J Biol Chem* **275**, 2686–2692.

Zhang ZH & Solomon AK (1992). Effect of pCMBS on anion transport in human red cell membranes. *Biochim Biophys Acta* **1106**, 31–39.

Acknowledgements

We are especially grateful to Mrs Kornelia Anders for her excellent help with the preparation of ghosts and her general technical assistance.